IET Image Processing

Research Article

IET Journals
The Institution of Engineering and Technology

Empirical wavelet transform-based fog removal via dark channel prior

ISSN 1751-9659
Received on 5th May 2019
Revised 14th November 2019
Accepted on 15th January 2020
E-First on 11th April 2020
doi: 10.1049/iet-ipr.2019.0496
www.ietdl.org

Manas Sarkar[1], Priyanka Rakshit Sarkar[1], Ujjwal Mondal[2], Debashis Nandi[3] ✉

[1]*Department of Instrumentation and Control Engineering, Haldia Institute of Technology, Haldia, India*
[2]*Department of Applied Physics, Calcutta University, Kolkata, India*
[3]*Department of Computer Science and Engineering, National Institute of Technology, Durgapur, India*
✉ *E-mail: debashis@cse.nitdgp.ac.in*

Abstract: Haze and fog removing from videos and images has got massive concentration in the field of video and image processing because videos and images are severely affected by fog in tracking and surveillance system, object detection. Different defogging techniques proposed so far are based on polarisation, colour-line model, anisotropic diffusion, dark channel prior (DCP) etc. However, these methods are unable to produce output image with desirable quality in the presence of dense fog and sky region. In this study, the authors have proposed a novel fog removal technique where DCP is applied on the low-frequency component of empirical wavelet transformation coefficients of the foggy input image. They apply unsharp masking on wavelet coefficients of the embedded wavelet transformed image for improving the sharpness of the output image. Later contrast limited adaptive histogram equalisation technique is used as a post-processing task to the inverse transformed image for producing the sharp and high contrast output. Finally, the colour and intensity of the contrast-enhanced image are uplifted through S-channel and V-channel gain adjustment. The proposed method provides significant improvement to the overall quality of the output image compared to contemporary techniques. The quantitative and qualitative measurements confirm the claims.

1 Introduction

Many systems in computer vision applications, like navigation, tracking, and surveillance, object detection etc. have suffered from fog and haze since fog in the atmosphere degrades the visibility in terms of sharpness, intensity, contrast, and colour quality. The information of the scene objects is lost due to such degradation of quality. It makes the visibility of objects of a scene very poor. For example, driving in foggy weather in hill stations is difficult since the hilly roads are steep, and the possibilities of accidents are high. In most computer vision applications, we require a haze-free image or video as an input to recognise the objects and/or measure the depth (a distance of the objects from the camera system) by utilising the input images or video frames [1]. Hence many researchers have imposed their interest in developing fog/haze removal techniques [1–8].

In the atmosphere, fog is generated due to absorption, reflection, and scattering of atmospheric light, which come from scene objects through water droplets and other suspended atmospheric particles [1, 7]. So the received irradiance from scene objects gets attenuated. The amount of fog present in an image is a function of the scattering coefficient and depth of the scene objects. Defogging or dehazing is a technique of elimination of fog or haze from video frames or images for improving the scene visibility in terms of intensity, colour, contrast, and other parameters.

Since the fog is a function of depth and scattering coefficient, it becomes a challenging task for a researcher to explore these unknown parameters from the foggy image frames. Generally, two different types of dehazing techniques are used in practice depending on the image frame numbers: (i) based on a single frame [1, 2, 5–7, 9, 10]; and (ii) based on multiple frames [3, 4]. Only a single frame of a test image of a scene is used for single-frame defogging techniques, whereas in the case of multi-frame techniques, the fog is removed by using multiple frames of the same image scene. The acceptance of the single-frame defogging method is more because no prior information is required from the reference image like multi-frame defogging techniques. Since the last decade, many fog and haze removal techniques have been proposed. However, most of them suffer from the following limitations: (a) They fail to provide information about the whole scene in the presence of thick fog and sky region. (b) They only enhance visibility without concentrating on the improvement of the depth of the scene [10]. (c) In some cases, the colour quality, sharpness, contrast, and intensity are not correctly adjusted together. Tarel and Hautiere [2] propounded an idea of visibility restoration by assuming the colours of small objects with low saturation values. The algorithm was mainly proposed for real-time use. However, its performance depends on the adjustment of many parameters. He *et al.* [1] proposed an innovative single-image fog removal technique with a new idea of dark channel prior (DCP). The DCP is built with very low-intensity pixels or dark pixels of the colour channels of an image. The depth of the fog can be estimated easily by this method. However, it becomes inefficient to provide good results when the brightness of the scene object and the intensity of atmospheric light are approximately at the same level. Anisotropic diffusion and histogram stretching-based fog removal technique have been proposed by Tripathi and Mukhopadhyay [7]. Anisotropic diffusion is used for the refinement of the air-light map from the novel DCP method. The depth of the fog does not have dependency on parameters and constants. Fattal [8] developed a defogging method for colour image depending on the local colour-line model. The intensity values of pixels of small image patches are distributed in one dimension, which is shown by the proposed model. The transmission map is estimated using this colour-line model. Variable gamma correction factors are used for the accurate restoration of an image. This method is based on some specific assumptions and does not work well in the sky region. Kyungil *et al.* [6] introduced a discrete wavelet transform (DWT) with DCP-based fog removal method, which performs different operations in different bands. In this method, the scene depth is estimated by DCP, and contrast limited adaptive histogram equalisation (CLAHE) improves the contrast in the V channel. High- and low-frequency image components are used to reduce the noise and enhance image sharpness. Sometimes, the defogged output encountered artefacts due to the operations on high-frequency components. Md. Imtiyaz and Arun [5] proposed a method of fog removal, which uses DCP as a pre-processing and weighted least

square (WLS) along with a high dynamic range (HDR) as a post-processing technique. The post-processing approach further improves the output image quality. However, the results in this method sometimes become brighter than the typical or standard image. By observing the limitations of the prior works, we become motivated to propose a new and novel fog/haze removal technique to obtain better performance concerning the state-of-the-art.

In this paper, we have introduced empirical wavelet transformation (EWT) along with the DCP-based fog removal technique to extract more information about the objects of a scene by adaptively analysing the frequency domain. To achieve the optimum visibility of objects in the final output image, we take care of the important parameters like intensity, sharpness, contrast, colour, and resolution of the scene image. Recently, a new and emerging image decomposition technique EWT [11, 12] has been proposed by Gilles *et al.* and used in several applications for processing the signal and image [13]. In EWT, the decomposition of the different frequency components is performed adaptively by investigating the texture of the image pixels. It adapts the information variations through the Fourier spectrum of the image signal, and accordingly, different modes or components of the image signal are generated. After obtaining different categories of information in different modes, we may take necessary actions on each mode to reveal the real information about the objects and to improve the overall quality and visibility of the scene image. Different operations are performed on different decomposed parts to obtain definite improvement on low- to high-frequency ranges of the image. Depth of the fog in a foggy vision is estimated by using the DCP technique [1] on the low-frequency zone of EWT coefficients (approximation coefficients). Halo effects and block artefacts from the scene transmission map are removed by using edge-preserving guided filter [14, 15]. Unsharp Masking (USM) [16–18] is performed on the high-frequency regions to improve the sharpness and resolution of the defogged output. CLAHE [19, 20] is applied to the whole image to improve the contrast of the output. The final output is obtained by enhancing the intensity and colour in the S and V channels of the image obtained from the previous step.

2 Brief review of previous works

Tarel and Hautiere [2] presented a defogging technique that may be used in the in-vehicle camera. This algorithm can restore the image visibility successfully by preserving the edges and other parameters. At the same time, the processing time of this approach is also fast. It works both for colour and grey images. By the assumption of low saturation colour of small scene objects, the algorithm is developed. Some parameters like image restoration, atmospheric veil inference, smoothing, and tone mapping, control the performance of the whole algorithm. The restored defogged image may be represented as follows:

$$R(x,y) = \frac{I(x,y) - V(x,y)}{1 - (V(x,y)/(I_s))} \tag{1}$$

where $V(x,y)$ is atmospheric veil and I_s is the sky intensity. This method is not efficient to restore the original colour and also unable to handle dense fog.

He *et al.* [1] proposed a 'dark channel prior' for removing fog from a foggy image. The DCP is a type of statistical measurement of a fog-free image. It works based on the investigation of the local patches of a fog-free image. Most of the local patches of a fog-free image must have some low-intensity value pixels or dark pixels in one of the three colour channels (R, G, and B). In a visual sense, the intensity values of the dark channel give a rough approximation of the depth of fog. By using this principle, along with the foggy image model given in (3), they estimated the thickness of fog and the transmission map. The transmission map is estimated by them is given as

$$\tilde{t}(x) = \omega \min_{y\epsilon\Omega(x)} \left(\min_{c} \frac{I^c(y)}{A^c} \right) \tag{2}$$

where $\tilde{t}(x)$ is the transmission and $\min_{y\epsilon\Omega(x)} (\min_c (I^c(y)/(A^c)))$ is the dark channel of the foggy image. If we put $\tilde{t}(x)$ in (3), the generated image may suffer from defogging artefacts. These artefacts may be removed by refining the transmission map through the soft matting process by using the matting Laplacian matrix. Sometimes, this method may be inefficient to estimate dense fog and unable to determine the depth of the sky region in the image.

Tripathi and Mukhopadhyay [7] have used anisotropic diffusion for refining air-light along with the DCP method to make the image visible and clear. However, they applied DCP on HSI colour space of the image to reduce the computational load. However, the algorithm may also be adapted to the RGB colour space of an image. The performance of this algorithm is satisfactory to a certain level in terms of high contrast gain and low saturated pixels.

A colour image defogging technique based on a local colour-line model is developed by Fattal [8]. It shows a one-dimensional (1D) distribution of intensity values of small image patches by availing the advantages of a generic regularity in image pixels. The identified patches which do not come under the local colour-lines are discarded. The proposal of excited GMRF (Gauss–Markov-Random-Field model) model works for the better solution of the transmission in isolated pixels. For accurate colour image restoration, variable gamma correction factors are used. However, the method finds colour-line using some specific assumptions, and sometimes it is challenging to set the conditions of identifying patches by obeying the model assumption.

Md. Imtiyaz and Arun [5] proposed a method that uses the DCP approach as a pre-processing technique and WLS along with HDR approaches as post-processing technique. This algorithm improves the colour and contrasts of an input image and also preserves the edges. Edge preservation is done via WLS filter.

Kyungil *et al.* [6] have introduced a DCP-based defogging technique using the wavelet domain. Different ranges of frequency components of an image hold different structural information as well as many unique features. By utilising this fact, image haziness, visibility, and overall quality have been improved. Discrete wavelet transformation (DWT) [21] is used soon after getting the fog-free image by DCP to reduce the noise and improve the sharpness. CLAHE is applied to the hue, saturation, value (HSV) formatted DCP output for enhancing the contrast of the final production.

3 Proposed algorithm

On account of these above limitations, we have developed a novel fog removal technique based on EWT and DCP, which can provide better results with respect to the recently proposed algorithm in the literature. The block diagram representation of the proposed method is shown in Fig. 1.

The proposed technique uses the same fog model used in [1] which is represented as:

$$O(x) = J(x)*t(x) + A(1 - t(x)) \tag{3}$$

where $O(x)$ is the intensity of an observed image in foggy condition, $J(x)$ is the fog-free image intensity or scene radiance, $t(x)$ is the medium transmission, A is global atmospheric light. As per this model, mainly two factors are responsible for the generation of atmospheric fog:

(i) Direct attenuation.
(ii) Air light.

In a foggy image, as the depth of the scene increases, the scene radiance is exponentially reduced. The scene-depth is related with transmission. So to construct a fog-free image from its foggy version, i.e. to recover (x), we need to estimate A and $t(x)$.

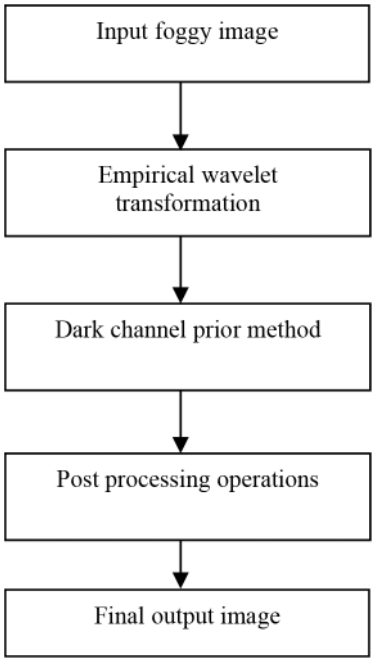

Fig. 1 *Block diagram of proposed algorithm*

3.1 EWT for image decomposition and image defogging

In the proposed model, we first apply EWT on a foggy image to decompose it. EWT is a new idea for decomposing a signal having the following properties [11, 12]:

(a) Adaptive in nature.
(b) Proper frequency band selection capability.
(c) Speed of operation.
(d) Efficiency.

It identifies the location of the signal information from the Fourier spectrum through an adaptive filtering process. The adaptive filters produce different modes or bands of the signal based on wavelets.

The adaptive nature in band selection based on signal information in EWT makes it more suitable over DWT for many applications. We utilise this property of the EWT to improve the performance of the new defogging technique.

EWT consists of the following operations:

(i) Representation of an input signal into a frequency domain using pseudo polar FFT.
(ii) Segmentation of the Fourier spectrum adaptively based on signal information.
(iii) Construction of the scaling and wavelet functions based on the segmented frequency values.

In this work, considering an image as a 2D signal, we follow the following notations:

(i) Any spatial point, $x = (x_1, x_2)$.
(ii) Any point in frequency plane, $\omega = (\omega_1, \omega_2)$.

In EWT method, we divide the frequency range which is restricted to $\omega\epsilon[0, \pi]$ into N partitions. This operation generates the boundaries Ω or $\{\omega^n\}_{n=0 \text{ to } N}$ as shown in Fig. 2, where $\omega^0 = 0$ to $\omega^N = \pi$. Based on (4) and (5) the empirical wavelets $B = \left\{\phi_1(x), \{\psi_n(x)\}_{n=1}^{N-1}\right\}$ are built. Here $\phi_1(x)$ represents the scaling function and $\psi_n(x)$ represents the empirical wavelets. Fig. 2 shows the empirical Fourier line decomposition of the signal. It is observed in Fig. 2 that, the overlapping between two consecutive frames can be avoided by taking a proper value of γ [11, 12]. The values of wavelet function depend on the adjustment parameter γ which is shown in (4) and (5). Hence, by choosing the proper value of γ, a certain gap between two consecutive bands or frames can be maintained and accordingly the boundaries between the consecutive sub-band images can be handled.

In the EWT method, the Fourier transformation of a signal is as follows:

$$F_{1,x}(\phi_1)(\omega) = \begin{cases} 1 \\ \text{if} |\omega| \le (1-\gamma)\omega^1 \\ \cos\left[\frac{\pi}{2}\beta\left(\frac{1}{2\gamma\omega^1}(|\omega| - (1-\gamma)\omega^1)\right)\right] \\ \text{if}(1-\gamma)\omega^1 \le |\omega| \le (1+\gamma)\omega^1 \\ 0 \\ \text{otherwise} \end{cases} \tag{4}$$

and

$$F_{1,x}(\psi_n)(\omega) = \begin{cases} 1 \\ \text{if}(1+\gamma)\omega^n \le |\omega| \le (1-\gamma)\omega^{n+1} \\ \cos\left[\frac{\pi}{2}\beta\left(\frac{1}{2\gamma\omega^{n+1}}(|\omega| - (1-\gamma)\omega^{n+1})\right)\right] \\ \text{if}(1-\gamma)\omega^{n+1} \le |\omega| \le (1+\gamma)\omega^{n+1} \\ \sin\left[\frac{\pi}{2}\beta\left(\frac{1}{2\gamma\omega^n}(|\omega| - (1-\gamma)\omega^n)\right)\right] \\ \text{if}(1-\gamma)\omega^n \le |\omega| \le (1+\gamma)\omega^n \\ 0 \\ \text{otherwise} \end{cases} \tag{5}$$

where $F_{1,x}$ represents the Fourier transform of the signal. β is an arbitrary function satisfying the following properties:

$$\beta(x) = 0, \quad \text{if } x \le 0$$

$$\beta(x) = 1, \quad \text{if } x \ge 1$$

$$\text{and} \quad \beta(x) + \beta(1-x) = 1, \quad \forall x \in [0, 1] \tag{6}$$

γ is an adjustment parameter used to maintain a gap between two consecutive bands and to avoid overlapping between two frames. Different wavelet frames are generated as the outputs of different bandpass filters, which are shown in (4) and (5). These formations

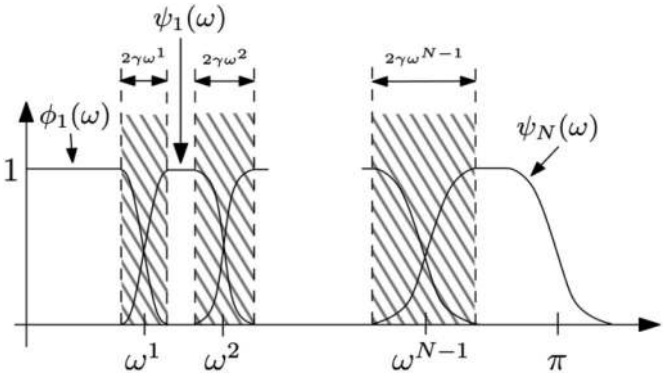

Fig. 2 *EWT boundary generation and filter construction*

of wavelet are done for 1D signals. The same formulations can be extended to 2D signals by assuming the independent variables of the functions as 2D vectors. So, the 2D empirical Littlewood-Paley transform of an input image f is given by

$$W_f^{\mathrm{ELP}}(n,x) = F_2^*(F_2(f)(\omega)(F_2(\psi_n)(\omega)))) \tag{7}$$

For the approximation coefficients, it will be

$$W_f^{\mathrm{ELP}}(0,x) = F_2^*(F_2(f)(\omega)(F_2(\phi_1)(\omega)))) \tag{8}$$

The output image is obtained by inverse Littlewood-Paley transform which is given by

$$f(x) = F_2^*\left(F_2\left(W_f^{\mathrm{ELP}}\right)(0,\omega)F_2(\phi_1)(\omega) + \sum_{n=1}^{N-1} F_2\left(W_f^{\mathrm{ELP}}\right)(n,\omega\right) F_2(\psi_n)(\omega)\Bigg) \tag{9}$$

where F_2 and F_2^* represent the Fourier transform and the inverse Fourier transform, respectively.

The order of the wavelet N is determined from the number of most important maxima in the magnitude of the Fourier spectrum of the input signal. The rule of the selection of N as follows.

Let us suppose that $P_1,\ P_2,\ \ldots P_M$ represent M number of peaks (maxima) detected form the Fourier spectrum of an input signal. Then we sort the peaks in descending order such that $P_1, \geq P_2 \geq \cdots \geq P_M$. Now we keep those maxima which are more significant than some amount of the difference of highest peak and smallest peak. The formula of the threshold used for the selection of these important peaks or maxima is $P_M + \alpha(P_1 - P_M)$. Since it is seen that the consistent results are obtained if the value of α is taken around 0.3 and 0.4, we have taken $\alpha = 0.3$. In this way, we have estimated the order of the wavelets or the value of N.

In our proposed defogging algorithm, the Fourier support $[0,\ \pi]$ of the foggy input image $f(x)$ is segmented into N contiguous segments; where ω^n represent the limits between each segment with $\omega^0 = 0$ and $\omega^N = \pi$. Hence, if we denote each by B_n, where $B_n = \left[\omega^{n-1}, \omega^N\right]$, then we can write

$$\bigcup_{n=0}^{N-1} B_n = [0,\ \pi] \tag{10}$$

The transition region of width $2\tau_n$ between two successive bands are represented by T_n. The empirical wavelets are particularly the bandpass filters on each B_n. So the wavelet bases are used to extract the segmented bands. Moreover, there is a systematic mathematical theory for decomposition of signals through EWT, which uses wavelet bases. This mathematical theory may be used for developing the theory of fog/haze removal.

In our proposed algorithm, for an input foggy/haze image, we find out the wavelets $W_f^{\mathrm{ELP}}(0,x)$ and $W_f^{\mathrm{ELP}}(n,x)$ corresponding to each segment B_n. Here $W_f^{\mathrm{ELP}}(0,x)$ gives the approximation coefficients and $W_f^{\mathrm{ELP}}(n,x)$, $n = 1,2,\ldots N-1$, gives the detail coefficients. Now we apply the DCP on $W_f^{\mathrm{ELP}}(0,x)$ and other image enhancement operations on $W_f^{\mathrm{ELP}}(n,x)$ to obtain processed wavelet coefficients $\hat{W}_f^{\mathrm{ELP}}(0,x)$ and $\hat{W}_f^{\mathrm{ELP}}(n,x)$. Finally, we obtain the processed image $\widehat{f}(x)$ by applying inverse EWT as follows:

$$\hat{f}(x) = F_2^*(F_2(\hat{W}_f^{\mathrm{ELP}})(0,\omega)F_2(\phi_1)(\omega) + \sum_{n=1}^{N-1} F_2(\hat{W}_f^{\mathrm{ELP}})(n,\omega)F_2(\psi_n)(\omega)) \tag{11}$$

We observe that the fog/haze is almost removed from the processed image and a significant improvement has been achieved.

The advantage of this empirical approach is to keep together some information. Otherwise, that would be split in the case of dyadic filters. The EWT may provide an adaptive representation of sub-band decomposition in which the wavelet bases are generated according to the information contained within the image. Due to this signal information-dependent adaptive nature of decomposition, we predict that most of the fog/haze information will be concentrated within the approximation sub-band. Hence, the application of the DCP to the sub-image of the approximation sub-band may help to reduce more amount of fog/haze from the input image. This idea has motivated us to give stress on EWT in the proposed fog/haze removal algorithm.

3.2 Fog depth estimation using DCP and determination of scene radiance

The DCP is a type of statistical measurement of a fog-free image. It works depending on the observation of the local patches of a fog-free image. It is proposed that most of the local patches of a fog-free image must have some low-intensity value pixels or dark pixels in one of the three colour channels [1]. Roughly the intensity of DCP is approximated by fog thickness. Hence we may estimate the thickness or depth by the use of DCP principle and the fog model. The dark channel is defined and rigorously treated by He *et al.* [1]:

$$J^{\mathrm{Dark}}(x) = \min_{y\epsilon\Omega(x)} \left(\min_{c\epsilon\{R,G,B\}} J^c(y)\right) \tag{12}$$

where J^c and $\Omega(x)$ indicate the colour channel of $J(x)$ and local patch of centre x, respectively. Fog depth is estimated by DCP and the transmission $\tilde{t}(x)$ is calculated by using (13)

$$\tilde{t}(x) = \mu \min_{y\epsilon\Omega(x)} \left(\min_{\mathrm{c}} \frac{I^c(y)}{A^c}\right) \tag{13}$$

where $\mu = (0,1)$. The value of μ indicates the amount of haze that we want to remove. Higher value of μ implies the higher amount of haze removal. If we take $\mu = 1$, the haze will be completely removed, but in that case we may lose the feeling of depth and it

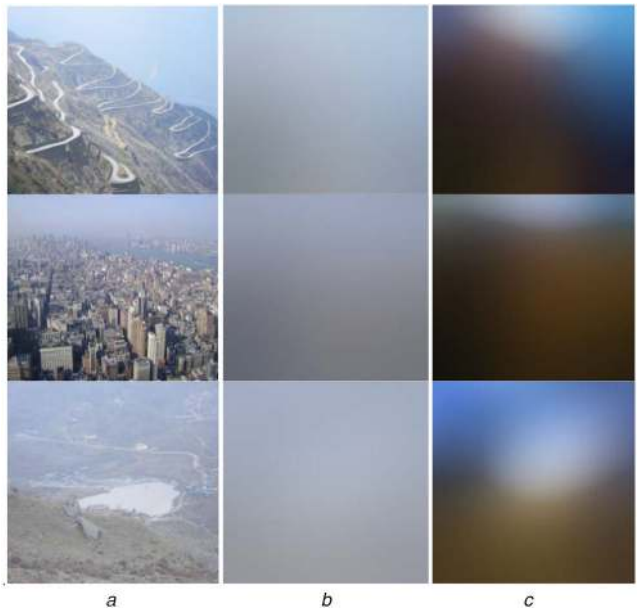

Fig. 3 *Low-frequency bands of different foggy images before and after applying DCP*
(a) *Foggy images,* ***(b)*** *Spatial domain of low-frequency bands,* ***(c)*** *Outputs after applying DCP*

may seem unnatural. So it is customary to keep small amount of haze willingly for the distant objects by taking = 0.95. However, we cannot permit more haze to pass in the output image by taking smaller values of μ. Most of the works on haze removal have taken $\mu = 0.95$ [1, 5] to achieve near optimal performance. The transmission map obtained from (13) must be refined because it holds constant value in patch, and it contains halo effects and block artefacts that appear in the final result. Guided filter [14, 15] is used for this purpose, which is fast, edge-preserving, and smooth operator. It can give better and satisfactory results close to the edges compared to other filters like Laplacian [1], bilateral etc. The distribution function of image transmittivity is given through soft matting. After getting refined transmission, scene radiance or defogged output is estimated. The guided filter operation is expressed as:

$$t(x) = \frac{1}{P}\sum_{k|x\in w_k}(a_k I_x + b_k) \tag{14}$$

where a_k and b_k are linear coefficients determined by the input image and by the estimated rough transmission. P is the number of pixels in the window w_k. After refinement of transmission map, defogged component is achieved as:

$$J(x) = \frac{O(x) - A}{\max(t(x), t_0)} + A \tag{15}$$

Always, some amount of noise is present in recovered scene radiance $J(x)$. For this reason, a lower bound value of transmission $t(x)$ is set to be 0.1 which is denoted by t_0.The above technique is applied on the low-frequency band image $W_f^{\mathrm{ELP}}(0, x)$ for reducing the fog and the reconstructed output $\hat{W}_f^{\mathrm{ELP}}(0, x)$ is generated.

Fig. 3 shows some image frames; the spatial domain of their low-frequency band $W_f^{\mathrm{ELP}}(0, x)$ and the results after applying the DCP on the spatial domain of the low-frequency bands.

3.3 Sharpness enhancement with preserved edge information using USM

USM [16] performs its operation based on the high pass filter when a test image is added to the same scaled image. It deals with edges and other high-frequency components to enhance the edges and fine details of the signal. It also improves the visual quality of the image, along with brightness and clarity. We perform USM on the image segments $W_f^{\mathrm{ELP}}(1, x)$ to $W_f^{\mathrm{ELP}}(N-1, x)$ for increasing the sharpness and preserving the edge information of the final output. $W_f^{\mathrm{ELP}}(1, x)$ to $W_f^{\mathrm{ELP}}(N-1, x)$ represent the groups of wavelet coefficients that correspond to gradually higher frequency segments. Each frequency segment contains a band of frequencies, some of which are lower than the others. When we apply the USM on the wavelet coefficients corresponding to a higher frequency segment, the higher frequency components are enhanced with respect to the lower frequencies of the that frequency segment. The application of USM enhances the edges and the fine details of the image under consideration. Consequently, the overall quality of the image is improved. This USM generates a new set of segments $\hat{W}_f^{\mathrm{ELP}}(1, x)$ to $\hat{W}_f^{\mathrm{ELP}}(N-1, x)$.

3.4 Post-processing operations

The defogged image may suffer from poor contrast, colour, and intensity. Hence it is required to adjust the contrast of the output image for better visibility. We use CLAHE [19, 22] for enhancing the contrast of the final defogged image. The CLAHE technique enhances the local contrast as well as the edges in an image.

The colour and intensity of the contrast-enhanced defogged image may be uplifted through the adjustment of colour S-channel and intensity in V-channel by choosing proper gain in both the cases.

4 Simulation results and performance analysis

The simulation and experiments are carried out in MATLAB 15 software on windows 10-based Personal Computer having 2.8 GHz Intel core i-5 processor. We have defogged several foggy image frames by using the proposed algorithm as well as some recently developed defogging techniques and compared the outputs to assess the relative performance of the proposed method with the others. The performance is assessed through quantitative and subjective assessment techniques. Subjective assessment is performed based on the pictorial view of the results. We perform quantitative measurement by computing few quantitative quality metrics like (a) Contrast Gain (*CG*) [7, 20], (b) Colourfulness Index (*CI*) [23, 24], (c) Colour Information Entropy (*CIE*) [5], and (d) No reference image quality assessment or image anisotropy (*AQI*) [25–27]. It is observed that the proposed algorithm produces better outputs in most of the cases in both assessment procedure concerning the other techniques.

Contrast gain (*CG*) is an important image quality assessment metric to measure the quality of the processed image. It is found that the contrast of the foggy image is lagged from the defogged

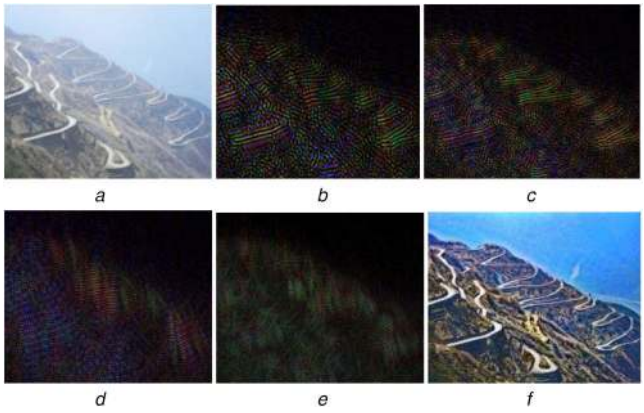

Fig. 4 *Image 'juluk':*
(a) Foggy image, ***(b)–(e)*** Different decomposed high-frequency image components, ***(f)*** Defogged output

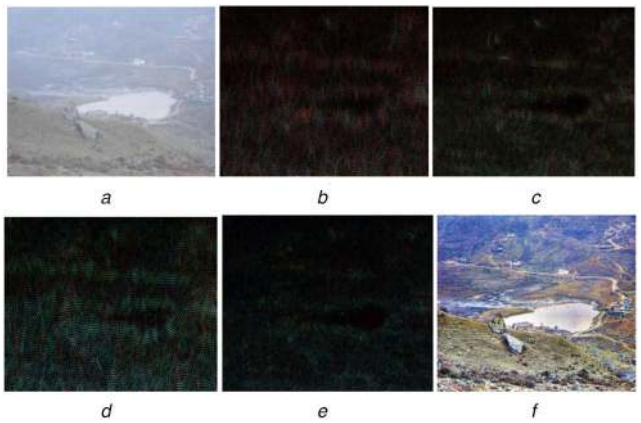

Fig. 5 *Image 'kupup lake'*
(a) Foggy image, ***(b)–(e)*** Different decomposed high-frequency image components, ***(f)*** Defogged output

one. Therefore, the higher value of *CG* implies a better quality image in terms of contrast because the *CG* is nothing but the difference of mean contrast between defogged output and input foggy image. It can be expressed as:

$$CG = C_{\mathrm{I,def}} - C_{\mathrm{I,fog}} \tag{16}$$

where $C_{\mathrm{I,def}}$ and $C_{\mathrm{I,fog}}$ are set to be the mean value of contrast of the fog-free output and the input foggy image of size $M \times N$, respectively. Mathematical representation of an image mean contrast is defined as:

$$C_{\mathrm{I}} = \frac{1}{MN} \sum_{J=0}^{N-1} \sum_{i=0}^{M-1} C(i, j) \tag{17}$$

where the contrast value at the pixel location (i, j) is indicated by $C(i, j)$.

One of the important features of an image is colour and proper selection of each colour ratio makes an image pleasant and clear. So, colour quality of defogged images after refinement is evaluated by Colourfulness Index (*CI*). The Colourfulness Index (*CI*) for an image is expressed as:

$$CI = \sigma_{\mathrm{rgyb}} + 0.3\mu_{\mathrm{rgyb}} \tag{18}$$

where

$$\sigma_{\mathrm{rgyb}} = \sqrt{\sigma_{\mathrm{rg}}^2 + \sigma_{\mathrm{yb}}^2} \tag{19}$$

and

$$\mu_{\mathrm{rgyb}} = \sqrt{\mu_{\mathrm{rg}}^2 + \mu_{\mathrm{yb}}^2} \tag{20}$$

σ stands for the standard deviation and μ shows the mean value of the image pixels. Higher value of *CI* implies high-quality performance.

CIE is used to find the information present in a colour image. As more information provides better visibility, a defogged image should have higher *CIE* than a fog affected image. Mathematically, *CIE* is defined as:

$$CIE = -\sum_{k=0}^{L-1} P_k \log_2(P_K) \tag{21}$$

where grey levels are counted by L and P_K is the probability associated with grey level k or histogram count.

No reference image quality assessment or image anisotropy (*AQI*) metric changes with noise and blur, which are essential parameters for quality analysis. This method does not require any reference image for sorting the images as per the image quality. In this regard, this method is very much useful because fog-free image does not have any reference image to compare. The generalised Rényi entropy is used to calculate the entropy on a local basis by associating a distribution for each pixel of a digital image. This is how the entropy histograms can measure the content of information present in an image. The higher value of AQI implies the better quality output.

Figs. 4*a–f* and Figs. 5*a–f* show the images for two different inputs at different levels of the proposed algorithm. Figs. 4*a* and *f* are the foggy input and the defogged output of 'juluk' image, whereas Figs. 5*a* and *f* are the foggy input and the defogged output of 'kupup lake' image. Figs. 4*b–e* and 5*b–e* show the different decomposed non-overlapping high-frequency image components for two different input images.

The outputs of different techniques are shown in Figs. 6–13 by the use of foggy images 'ny17', 'y16', 'y01', 'canon', 'forest', 'cliff', 'cones' and 'pumpkins', respectively.

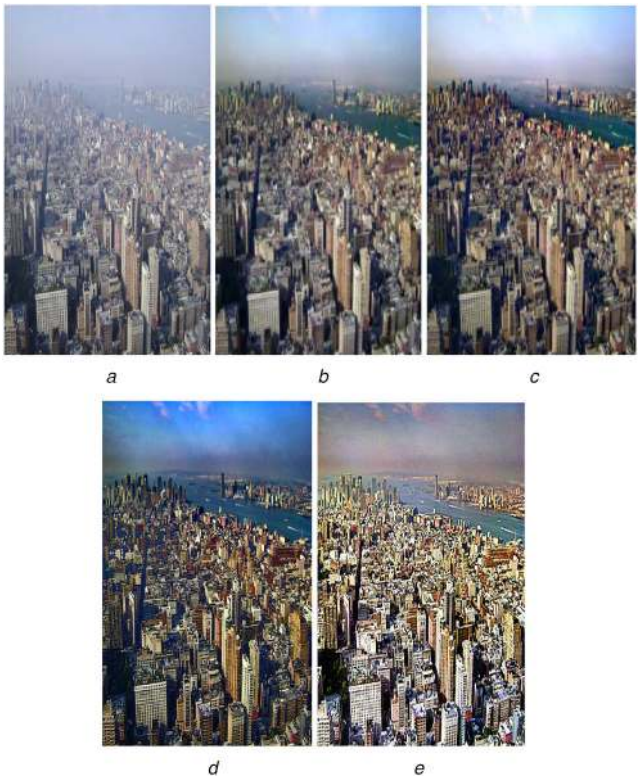

Fig. 6 *'ny17':*
(a) Foggy image, ***(b)*** He *et al.* [1], ***(c)*** Fattal [8], ***(d)*** Kyungil *et al.* [6], ***(e)*** Proposed method

Fig. 7 *'y16':*
(a) Foggy image, ***(b)*** He *et al.* [1], ***(c)*** Fattal [8], ***(d)*** Kyungil *et al.* [6], ***(e)*** Proposed method

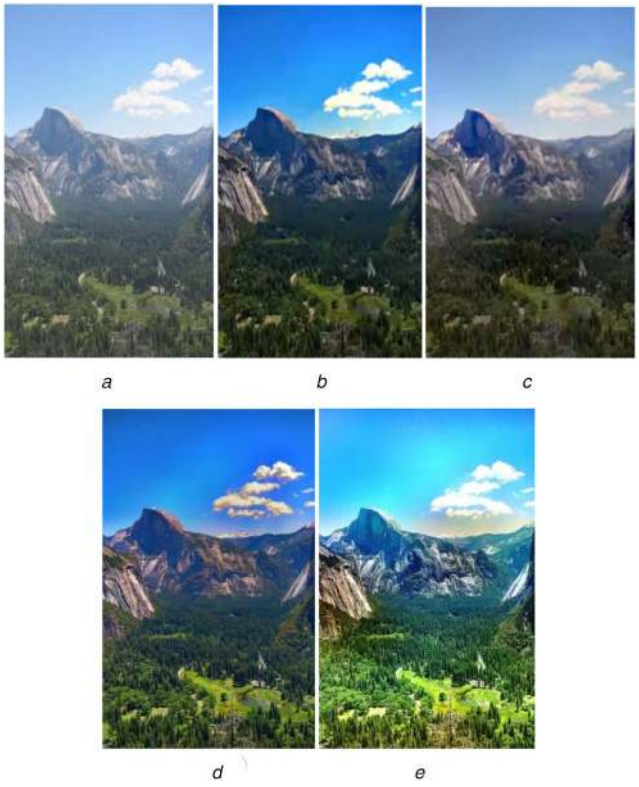

Fig. 8 *'y01':*
(a) Foggy image, ***(b)*** He *et al.* [1], ***(c)*** Fattal [8], ***(d)*** Kyungil *et al.* [6], ***(e)*** Proposed method

For analysing the performance of different algorithms quantitatively, we have estimated the quality metrics from the output images. The quality metrics obtained from different methods are tabulated in Tables 1 and 2. Table 1 shows the values of AQI and CIE, and Table 2 listed the values of CG and CI for different techniques and different images.

AQI gives a quantitative measure of the visual quality of an image. It measures the presence of degradation as a disturbing effect. The result shows that the value of this metric is better for the proposed method compared to the other methods considered. Coloured bar graphs in Fig. 14 are used to compare the AQI value in pictorial form.

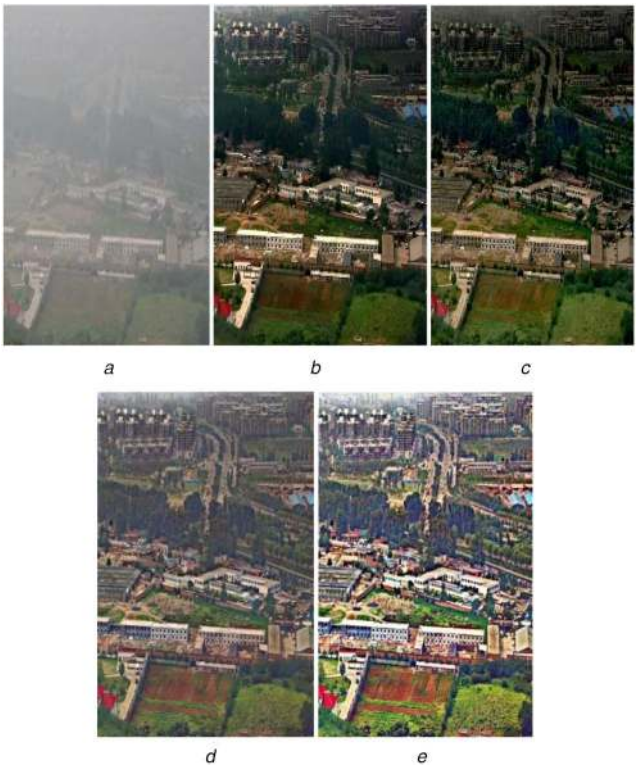

Fig. 9 *'canon':*
(a) Foggy image, ***(b)*** He *et al.* [1], ***(c)*** Fattal [8], ***(d)*** Kyungil *et al.* [6], ***(e)*** Proposed method

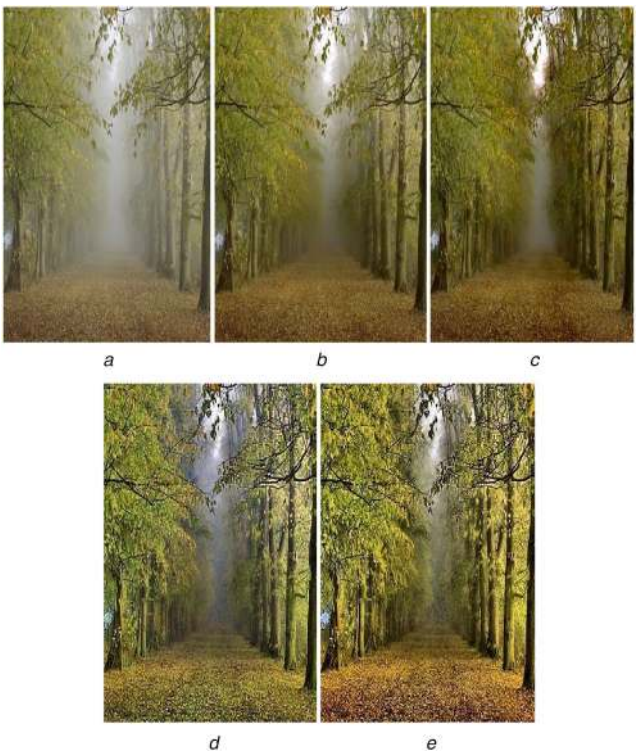

Fig. 10 *'forest':*
(a) Foggy image, ***(b)*** He *et al.* [1], ***(c)*** Fattal [8], ***(d)*** Kyungil *et al.* [6], ***(e)*** Proposed method

CIE is used to find the information present in a colour image. It measures the randomness to characterise the image texture. By taking an image histogram at each of the grey levels, the CIE value is determined. More value of CIE is obtained for an image that has more textural information. Out of eight test images ('ny17', 'y01','y16', 'forest', 'canon', 'cliff', 'cones' and 'pumpkins'), we achieve better CIE for five images ('forest', 'canon', 'cliff',

Fig. 11 *'cliff':*
(a) Foggy image, ***(b)*** He *et al.* [1], ***(c)*** Fattal [8], ***(d)*** Kyungil *et al.* [6], ***(e)*** Proposed method

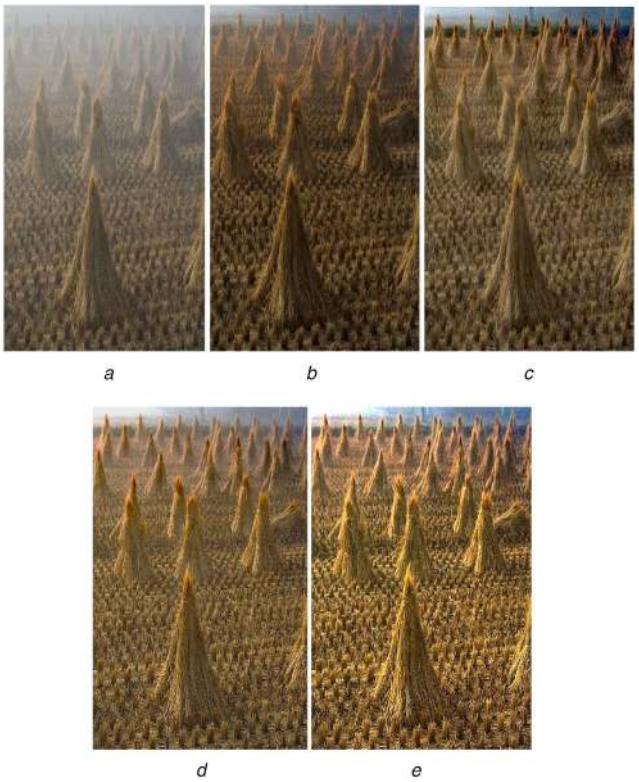

Fig. 12 *'cones':*
(a) Foggy image, ***(b)*** He *et al.* [1], ***(c)*** Fattal [8], ***(d)*** Kyungil *et al.* [6], ***(e)*** Proposed method

'cones' and 'pumpkins'). It is observed that the proposed algorithm gives lesser value for CIE for those test images which have large sky region. Three images (i.e. 'ny17', 'y01', and 'y16') have the sky region. Hence the value of CIE in the proposed method is lesser for these three images. Fog or haze and the sky region

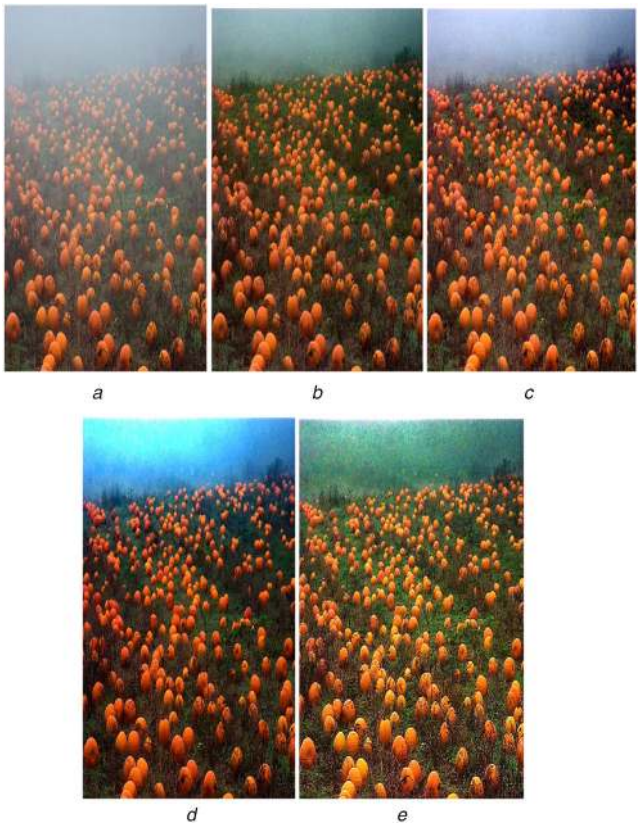

Fig. 13 *'pumpkins':*
(a) Foggy image, ***(b)*** He *et al.* [1], ***(c)*** Fattal [8], ***(d)*** Kyungil *et al.* [6], ***(e)*** Proposed method

Table 1 Comparison of AQI and CIE of different techniques

Images	Methods							
	He *et al.* [1]		Fattal [8]		Kyungil *et al.* [6]		Proposed method	
	AQI	CIE	AQI	CIE	AQI	CIE	AQI	CIE
ny17'	0.0769	7.8853	0.0715	7.6418	0.2093	7.617	0.2595	7.621
y01'	0.0419	7.4384	0.0273	7.5883	0.1011	7.658	0.1643	7.4583
y16'	0.0372	7.7625	0.0442	7.5922	0.0861	7.0822	0.1613	6.9293
canon7'	0.0679	5.1333	0.0871	6.3355	0.0982	6.9811	0.1374	7.6407
forest'	0.0488	6.5888	0.0875	6.5321	0.1159	6.7325	0.204	6.7684
cliff'	0.0502	6.242	0.0949	6.449	0.0952	6.651	0.1024	7.134
cones'	0.0606	6.642	0.0557	6.712	0.1051	7.049	0.1556	7.16
pumpkins'	0.0651	6.769	0.0731	7.212	0.1223	6.561	0.165	7.331

Table 2 Comparison of CG and CI of different techniques

Images	Methods							
	He *et al.* [1]		Fattal [8]		Kyungil *et al.* [6]		Proposed method	
	CG	CI	CG	CI	CG	CI	CG	CI
ny17'	0.093	15.835	0.0808	22.201	0.173	16.902	0.179	26.075
y01'	0.086	14.514	0.0389	21.444	0.141	35.994	0.145	38.461
y16'	0.068	17.497	0.0215	17.49	0.149	27.521	0.152	28.472
canon7'	0.019	12.873	0.0217	18.013	0.135	14.462	0.147	19.374
forest'	0.0312	15.776	0.0352	16.971	0.122	25.796	0.141	27.011
cliff'	0.031	4.07	0.068	5.89	0.119	8.18	0.131	13.3
cones'	0.039	10.85	0.081	10.88	0.121	15.34	0.147	18.2
pumpkins'	0.049	25.17	0.076	28.23	0.115	31.34	0.131	34.31

(without any object) of an image are contained in the lower frequency part of the transformed image. Since atmospheric light and the sky region appear quite similar, and the DCP is applied to the low-frequency part of the transformed image, the algorithm assumes the sky region as fog. The application of DCP to the low-frequency components of the colour channels may create small artefacts in the sky region. The USM may also generate a small amount of false colours. These effects reduce the CIE value for the images, especially with the sky region in the proposed algorithm.

The value of the CG metric measures the visual quality in terms of contrast. The more the fog will be removed, the more the contrast will be achieved. Therefore, the higher value of the CG metric implies the better contrast and, consequently, the better the removal of fog. From the results, we see that the value of CG is

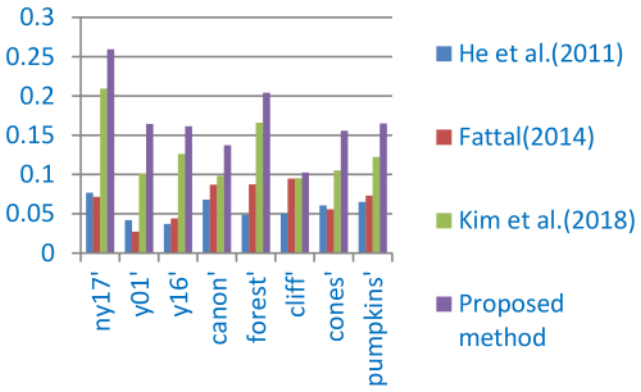

Fig. 14 *Comparison of AQI for different images among proposed and existing algorithms*

better for the proposed algorithm concerning the others, which implies the better performance of the proposed algorithm in terms of haze removal.

CI [24] measures the amount of different colours or the degree of colourfulness in an image. The more the colour of an image, the higher the value of CI. A higher value of CI carries more colour information, which enhances the visibility of an image. From the results, we observe that our proposed algorithm gives higher values of CI for all test images. It concludes that more colour information is present in the outputs of our proposed approach.

The above discussion reveals that the proposed algorithm provides an overall better performance both in terms of visual quality and quality metrics concerning contemporary algorithms.

5 Conclusions

This paper proposes a novel empirical wavelet transform and dark channel prior-based contrast- and colour-preserving image defogging algorithm. The method applies the DCP module along with the guided filter to the approximation coefficients in the empirical wavelet domain of the foggy image to remove fog. The sharpness of the output image has been improved through the application of USM on wavelet coefficients in the wavelet domain of the foggy image. The defogged image is rebuilt by performing an inverse empirical wavelet transform on the processed wavelet co-efficient. In the final stage, we apply local contrast enhancement to improve the contrast of the defogged image. The performance of the proposed algorithm has been compared with few recent defogging techniques through quality evaluation of the outputs. The results show that the overall visual quality for most of the output images of the proposed algorithm is better than the other recently proposed techniques in most of the cases. Hence, it confirms the superiority of the proposed algorithm concerning contemporary techniques.

6 References

[1] He, K., Sun, J., Tang, X.: 'Single image haze removal using dark channel prior', *IEEE Trans. Pattern Anal. Mach. Intell.*, 2011, **33**, (12), pp. 2341–2353

[2] Tarel, J.P., Hautiere, N.: 'Fast visibility restoration from a single color or gray level image'. Proc. 12th IEEE Int. Conf. on Computer Vision, Kyoto, Japan, 2009, pp. 2201–2208

[3] Schechner, Y.Y., Narasimhan, S.G., Nayar, S.K.: 'Instant dehazing of images using polarization'. Computer Vision and Pattern Recognition, in: Proc. IEEE Computer Society Conf., Kauai, HI, USA, 2001, vol. 1, pp. 325–332

[4] Kopf, J., Neubert, B., Chen, B., *et al.*: 'Deep photo: model-based photograph enhancement and viewing', *ACM Trans. Graphics*, 2008, **27**, (5), pp. 116:1–116:10

[5] Md. Imtiyaz, A., Arun, K.: 'Vision enhancement through single image fog removal', *Eng. Sci. Technol., Int. J.*, 2017, **20**, pp. 1075–1083

[6] Kyungil, K., Soohyun, K., Kyung-Soo, K.: 'Effective image enhancement techniques for fog-affected indoor and outdoor images', *IET Image Proc.*, 2018, **12**, pp. 465–471

[7] Tripathi, A.K., Mukhopadhyay, S.: 'Single image fog removal using anisotropic diffusion', *IET Image Proc.*, 2012, **6**, (7), pp. 966–975

[8] Fattal, R.: 'Dehazing using color-lines', *ACM Trans. Graph*, 2014, **28**, pp. 1–13

[9] Wang, Y., Fan, C.: 'Single image defogging by multiscale depth fusion', *IEEE Trans. Image Process.*, 2014, **23**, (11), pp. 4826–4837

[10] Tan, R.: 'Visibility in bad weather from a single image'. Proc. IEEE Conf. Computer Vision and Pattern Recognition, Anchorage, AK, USA, 2008, pp. 1–8

[11] Gilles, J.: 'Empirical wavelet transform', *IEEE Trans. Signal Process.*, 2013, **61**, (16), pp. 3999–4010

[12] Gilles, J., Tran, G., Osher, S.: '2D empirical transforms. Wavelets, ridgelets, and curvelets revisited', *SIAM J. Imaging Sci.*, 2014, **7**, (1), pp. 157–186

[13] Dong, S., Yuan, M., Wang, Q., *et al.*: 'A modified empirical wavelet transform for acoustic emission signal decomposition in structural health monitoring'. *MDPI Sensors J.*, 2018, **18**, (5), pp. 1645–1662

[14] He, K., Sun, J., Tang, X.: 'Guided image filtering', in Daniilidis, K., Maragos, P., Paragios, N. (Eds.): '*Computer vision – ECCV 2010*', vol. **6311**, (Springer, Berlin, Heidelberg, Germany, 2010) pp. 1–14

[15] Xiao, C., Gan, J.: 'Fast image dehazing using guided joint bilateral filter', *Vis. Comput.*, 2012, **28**, pp. 713–721

[16] Jadwiga, R., Kendall, P., Donald, S.: 'Evaluation of digital unsharp masking and local contrast stretching as applied to chest radiographs', *IEEE Trans. Biomed. Eng.*, 1988, **35**, (10), pp. 817–827

[17] Ying, L, Ming, N.T., Keat, L.B.: 'A wavelet based image sharpening algorithm'. Int. Conf. on Computer Science and Software Engineering, Hubei, China, 2008, pp. 1053–1056

[18] Polesel, A., Ramponi, G., John, M.: 'Image enhancement via adaptive unsharp masking', *IEEE Trans. Image Process.*, 2000, **9**, (3), pp. 505–510

[19] Zuiderveld, K.: '*Contrast limited adaptive histogram equalization*' Graphic Gems IV. (Academic Press Professional, San Diego, 1994), pp. 474–485

[20] Economopoulos, T.L., Asvestas, P.A., Matsopoulos, G.K.: 'Contrast enhancement of images using partitioned iterated function systems', *Image Vis. Comput.*, 2010, **28**, (1), pp. 45–54

[21] Mallat, S.: 'A theory for multiresolution signal decomposition: the wavelet representation', *IEEE Trans. PAMI*, 1989, **7**, (11), pp. 674–693

[22] Abdullah-Al-Wadud, M., Kabir, Md.H., Dewan, M.A.A., *et al.*: 'A dynamic histogram equalization for image contrast enhancement', *IEEE Trans. Consum. Electron.*, 2007, **53**, (2), pp. 593–600

[23] Xu J. Choi, B.-D., Jung, S.-W., *et al.*: 'Image enhancement using two gamma-rescaling curves and multiscale Gaussian matrix'. Int. Conf. on Intelligent and Advanced Systems, Kuala Lumpur, Malaysia, 2007, pp. 709–713

[24] Hasler, D., Suesstrunk, S.E.: 'Measuring colorfulness in natural images'. *Electron. Imaging Int. Soc. Optics Photonics*, 2003, **2003**, pp. 87–95

[25] Gabarda, S., Cristóbal, G.: 'Image quality assessment through a logarithmic anisotropic measure', *SPIE Photonics Europe*, 2008, **7000**, pp. 1–11

[26] Callico, G.M., Lopez, S., Gabarda, S., *et al.*: 'Anisotropic quality measurement applied to H.264 video compression', *SPIE VLSI Circuits Syst. IV*, 2009, **7363**, pp. 1–12

[27] Gabarda, S., Cristóbal, G.: 'Blind image quality assessment through anisotropy', *J. Opt. Soc. Am. A*, 2007, **24**, pp. B42–B51